



Universiteit  
Leiden  
The Netherlands

## **Biophysical characterization of membrane protein-small molecule interactions**

Chen, D.

### **Citation**

Chen, D. (2015, March 4). *Biophysical characterization of membrane protein-small molecule interactions*. Retrieved from <https://hdl.handle.net/1887/32075>

Version: Corrected Publisher's Version

License: [Licence agreement concerning inclusion of doctoral thesis in the Institutional Repository of the University of Leiden](#)

Downloaded from: <https://hdl.handle.net/1887/32075>

**Note:** To cite this publication please use the final published version (if applicable).

Cover Page



Universiteit Leiden



The handle <http://hdl.handle.net/1887/32075> holds various files of this Leiden University dissertation

**Author:** Dan Chen

**Title:** Biophysical characterization of membrane protein-small molecule interactions

**Issue Date:** 2015-03-04

## Chapter 4

# Complementarity Between *in silico* and Biophysical Screening Approaches in Fragment-Based Lead Discovery Against the A<sub>2A</sub> Adenosine Receptor

D. Chen, A. Ranganathan, A. P. IJzerman, G. Siegal, J. Carlsson. Complementarity between *in silico* and biophysical screening approaches in fragment-based lead discovery against the A<sub>2A</sub> adenosine receptor. *J. Chem. Inf. Model.* 2013, 53, 2701-2714.

## ABSTRACT

Fragment-based lead discovery (FBLD) is becoming an increasingly important method in drug development. We have explored the potential to complement NMR-based biophysical screening of chemical libraries with molecular docking in FBLD against the A<sub>2A</sub> adenosine receptor (A<sub>2A</sub>R), a drug target for inflammation and Parkinson's disease. Prior to an NMR-based screen of a fragment library against the A<sub>2A</sub>R, molecular docking against a crystal structure was used to rank the same set of molecules by their predicted affinities. Molecular docking was able to predict four out of the five orthosteric ligands discovered by NMR among the top 5% of the ranked library, suggesting that structure-based methods could be used to prioritize among primary hits from biophysical screens. In addition, three fragments that were top-ranked by molecular docking, but had not been picked up by the NMR-based method, were demonstrated to be A<sub>2A</sub>R ligands. While biophysical approaches for fragment screening are typically limited to a few thousand compounds, the docking screen was extended to include 328,000 commercially available fragments. Twenty-two top-ranked compounds were tested in radioligand binding assays, and 14 of these were A<sub>2A</sub>R ligands with K<sub>i</sub> values ranging from 2 to 240  $\mu$ M. Optimization of fragments was guided by molecular dynamics simulations. The results illuminate strengths and weaknesses of molecular docking and demonstrate that this method can serve as a valuable complementary tool to biophysical screening in FBLD.

## 1. Introduction

The adenosine receptors belong to the family of G protein-coupled receptors (GPCRs) and are expressed both in the central nervous system (CNS) and the periphery. The four adenosine receptor subtypes ( $A_1$ ,  $A_{2A}$ ,  $A_{2B}$ ,  $A_3$ ) are responsible for a wide range of physiological processes by acting on different signaling pathways. The  $A_{2A}$  and  $A_{2B}$  adenosine receptors increase cAMP levels by coupling to  $G_s$  whereas the  $A_1$  and  $A_3$  subtypes signal via  $G_i$  and decrease cAMP levels.<sup>1</sup>  $A_{2A}$  adenosine receptor ( $A_{2A}R$ ) activation occurs in response to stress or cell damage and protects tissues by controlling inflammation. For this reason,  $A_{2A}R$  agonists are candidates for development of anti-inflammatory drugs.<sup>2</sup> In the CNS, the  $A_{2A}R$  is expressed in the basal ganglia and counter-balances the action of the  $D_2$  dopamine receptor. The two receptors form heterodimers in the cell membrane and  $A_{2A}R$  activation leads to a decrease in  $D_2$  dopamine receptor signaling.<sup>3</sup> Since Parkinson's disease is characterized by a loss of dopamine receptor activity,  $A_{2A}R$  antagonists have been studied intensively as drug candidates for Parkinson's disease and several compounds are currently in clinical trials.<sup>1</sup>

The rapidly increasing number of crystal structures for G protein-coupled receptors (GPCRs) has made structure-based approaches an attractive strategy for drug design against these pharmaceutically important targets.<sup>4,5</sup> Twelve high-resolution structures, with bound antagonists or agonists, have been determined for the  $A_{2A}R$  since the first one was solved in 2008.<sup>6-9</sup> Structure-based computational ligand discovery based on these structures has been surprisingly successful. Two recent molecular docking screens against these structures have resulted in the discovery of several novel  $A_{2A}R$  antagonists.<sup>10,11</sup> The "hit rates" in these screens, *i.e.* the percentages of active compounds among those selected for experimental evaluation, were 35 and 41%, which is remarkably good for virtual screening. Similar results were achieved in docking screens against the  $\beta_2$  adrenergic<sup>12,13</sup>,  $D_3$  dopamine<sup>14</sup>, CXCR4<sup>15</sup>, and  $H_1$  histamine receptors<sup>16</sup>, which

further demonstrated the potential for structure-based drug design against these targets.

During the last decade, fragment-based lead discovery (FBLD) has steadily increased in popularity as an alternative to high-throughput screening (HTS).<sup>17,18</sup> The idea behind FBLD is to identify ligands that are about half the size of a drug. The increased coverage of chemical space in fragment libraries makes it possible to identify ligands from screens of only a few thousand compounds. Ligands from fragment screens are often of low affinity and lack selectivity, but can serve as a starting point for the development of new lead compounds. There are now a large number of successful examples of where fragment ligands identified by crystallography, surface plasmon resonance (SPR), or nuclear magnetic resonance (NMR) techniques have been used to generate high-affinity leads.<sup>17</sup> In fact, several compounds that originate from fragment screens are now in clinical trials and the first drug developed from FBLD was approved in 2011.<sup>19</sup> Fragment screens by NMR and SPR have also been carried out against GPCRs<sup>20,21</sup>, but this is still challenging because of difficulties in expressing these proteins in large quantities and their inherent instability outside the cell membrane. The use of *in silico* fragment-based screening has also been explored successfully, both for GPCRs<sup>16,22</sup> and soluble proteins<sup>23,24</sup>, but structure-based approaches have been questioned in this context<sup>25</sup>. Most molecular docking programs were developed for and benchmarked on drug-like compounds and thus may have difficulties to rank fragment ligands, which typically are of low affinity and only occupy subpockets of a binding site.

In this work, we explored fragment-based ligand discovery by carrying out two prospective docking screens against a crystal structure of the A<sub>2A</sub>R. The questions that we wanted to address were if molecular docking could be used to discover fragment ligands and if *in silico* methods in combination with biophysical screening methods could improve the efficiency of FBLD. In a first step, we computationally docked a set of 500 fragments to an A<sub>2A</sub>R crystal structure and ranked these compounds by affinity prior to an NMR-based screen of the same library. As the entire library was screened both *in silico* and experimentally, our

blind prediction of the results made it possible to evaluate the utility of molecular docking in FBLD. The comparison of the computational and experimental screens for the small fragment library showed that a majority of the orthosteric ligands were among the top-ranked compounds in the docking screen. In a second step, we extended the docking screen to include several hundred thousand commercially available molecules and tested top-ranked compounds experimentally. The results from this second screen allowed us to directly compare the fragment ligands and hit-rates from biophysical and structure-based computational screening approaches. Fourteen fragment ligands were discovered from the docking screen of this larger set of commercially available molecules. The structure-activity relationships (SAR) were explored for three novel A<sub>2A</sub>R ligands, guided by molecular docking and molecular dynamics (MD) simulations.

## **2. Results**

### **Ranking of a Fragment Library by Molecular Docking**

To test the performance of molecular docking in FBLD against the A<sub>2A</sub>R, parallel experimental and computational screens of an in-house library of 500 chemically diverse fragments were carried out. Prior to screening the fragment library using an NMR-based approach, the same set of molecules was computationally docked to the orthosteric site of an antagonist-bound crystal structure of the A<sub>2A</sub>R<sup>7</sup> using the program DOCK3.6<sup>26-28</sup>. Each molecule was sampled in, on average, 18700 orientations and 16 conformations. For each conformation that did not clash with the receptor, a physics-based scoring function was used to evaluate the complementarity of the fragment to the orthosteric site. The docking score was calculated from the sum of the receptor-ligand electrostatic and van der Waals interaction energy, corrected for desolvation of the ligand. The best scoring conformation for each fragment was used to rank these molecules by their predicted affinity to the A<sub>2A</sub>R. In total, 487 of the 500 fragments were successfully scored in the orthosteric binding site. The

average computation time per docked molecule was 10 seconds and, in total, only 80 minutes were required to screen the library.

### **Comparison of NMR-Based and Molecular Docking Screens of a Fragment Library**

Given the low affinity and specificity of typical fragment ligands, the molecular docking technique can be expected to have difficulties to rank such compounds by affinity. As every library molecule was tested for binding to the A<sub>2A</sub>R in the NMR-based screen, this gave a unique opportunity to assess the ability of molecular docking to discriminate between fragment ligands and experimentally verified non-binders.

The details of the methodology and experiments used to screen the fragment library against a thermostabilized mutant<sup>29</sup> of the A<sub>2A</sub>R by NMR have been presented in separate publications.<sup>21,30</sup> The results of the NMR-based screen of the fragment library are presented briefly in this section to enable a comparison to the docking predictions. Five hundred fragments, which were selected to represent a diverse set of molecules in terms of shape and chemistry<sup>31</sup>, were screened using the target immobilized NMR screening (TINS) technique<sup>30</sup>. The TINS screen resulted in 94 primary hits, which were further evaluated in radioligand displacement assays. Five molecules showed more than 30% displacement of the radioligand at 500  $\mu$ M and had well-behaved dose response curves, which corresponds to a hit-rate of 5% for the secondary screen. The five hits are shown in Table 1 and the K<sub>i</sub> values for these compounds ranged from 14 to 600  $\mu$ M. Another key metric for judging the potential of a fragment ligand is its ligand efficiency (LE). The LE value was calculated as  $RT\ln K_i/N_i$ , where N<sub>i</sub> is the number of heavy atoms.<sup>32,33</sup> The best LE value for the fragments discovered in the NMR-based screen was 0.53 kcal mol<sup>-1</sup> atom<sup>-1</sup>, which is in the range considered to be promising for further optimization (typically >0.35 kcal mol<sup>-1</sup> atom<sup>-1</sup>). Additional experiments revealed that 11 of the initial hits were either positive or negative allosteric modulators of the A<sub>2A</sub>R.<sup>21</sup> The remaining 79 hits were not found to displace radioligands from the orthosteric site or



allosterically modulate agonist or antagonist binding. These compounds were considered to be less potent fragment ligands, bind to regions that do not influence ligand binding to the A<sub>2A</sub>R orthosteric site, or be false positives.

To assess how well the docking was able to predict the results of the fragment screen, we generated receiver operating characteristic (ROC) curves for the identified ligands based on the predicted ranking for the compounds in the library. As the docking calculations only sampled fragment orientations in the orthosteric site, we did not expect to identify any allosteric ligands. For this reason, the ligands were divided into an orthosteric and allosteric group, which made it possible to directly compare the computational and NMR-based screening results. The ROC curves for the ortho- and allosteric ligands are shown in Figure 1. To quantify the ability of DOCK3.6 to identify ligands, we evaluated enrichment factors at different false positive rates (ROC\_EF<sub>x%</sub>, where x denotes the false positive rate).<sup>34</sup> For example, the ROC\_EF<sub>5%</sub> value was calculated as the fraction of true positives (ligands) identified when 5% of the false positives (non-binders) had been found in the ranked list divided by the fraction of false positives at that point, i.e. 0.05 in this case.<sup>35</sup> No enrichment of orthosteric ligands was found at 0.5%-1% false positive rate. One ligand was identified at a 2% false-positive rate, corresponding to an enrichment factor of 10. Four out of five orthosteric ligands were identified in the top 5% of the ranked database, which corresponded to an ROC\_EF<sub>5%</sub> equal to 16, i.e. a 16-fold improvement over random selection (Figure 1, red curve). The fifth orthosteric ligand, compound **4**, was not scored at all, which was due to the sampling scheme used in DOCK3.6. If the sampling parameters were (retrospectively) adjusted to determine a score for compound **4**, it was ranked as ~160 and would hence not have affected early enrichment. The enrichment of orthosteric ligands from the subset of 94 primary hits in the NMR-based screen was also calculated. The enrichment in this case was remarkably good, ranking four of the ligands in the very top of the database (Figure 1, gray curve, ROC\_EF<sub>0.5%</sub> = 120). Finally, as may have been expected, the enrichment of allosteric modulators was poor,

as reflected by that the ROC curve was closer to random enrichment (Figure 1, blue curve). Predicted binding poses for two of the orthosteric ligands from the NMR-based screen, compounds **1** and **5**, are shown in Figure 2. Both compounds interact with Asn253<sup>6,55</sup> of the A<sub>2A</sub>R, a residue that been shown to be critical for recognition of both agonists and antagonists.<sup>36</sup>

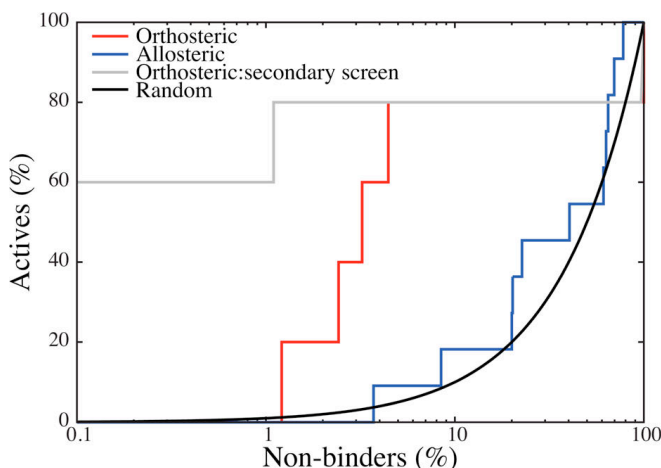


**Figure 1.** ROC curves for docking enrichment of orthosteric (red line) and allosteric (blue line) ligands discovered in the NMR-based screen. The enrichment of orthosteric ligands among the 94 molecules from the NMR-based screen that were selected for follow-up radioligand assays is also shown (grey line). The black line represents the curve expected from random enrichment.

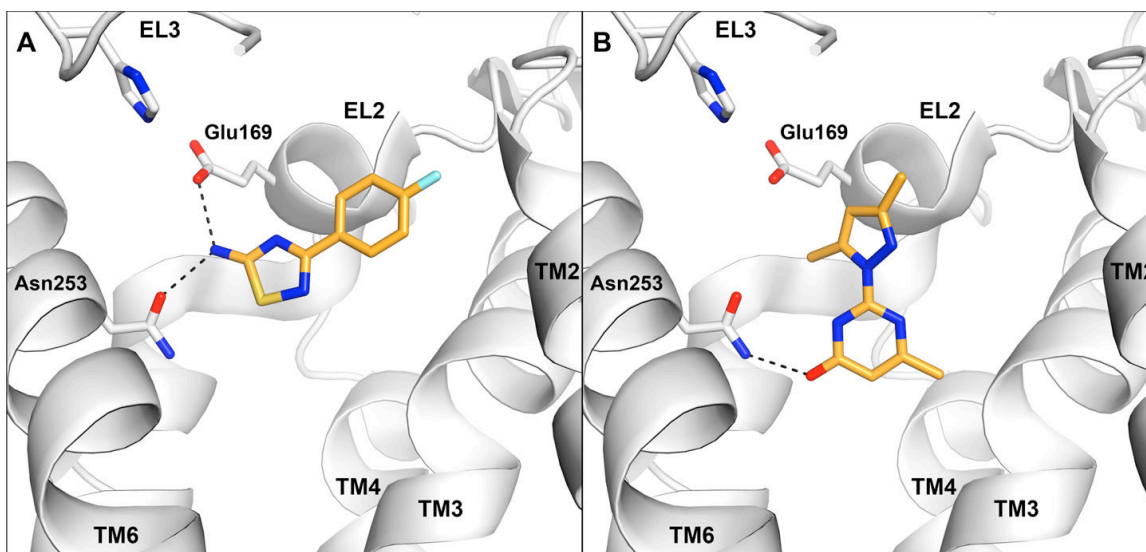


**Figure 2.** Predicted binding modes for two ligands (**1** and **5**) that were discovered in the NMR-based screen. The binding site is shown in white ribbons with selected side chains shown in sticks. The ligand is depicted with orange carbon atoms. Black dotted lines indicate hydrogen bonds. This figure was generated with PyMOL (version 1.4.1).

After assessing the ability of molecular docking to predict the results of the NMR-based screen, the top-ranked fragments from the docking calculations were analyzed in more detail. It was encouraging that 80% of the orthosteric ligands were among the top 50 compounds of the ranked library. However, this also suggested that there were 46 top-ranked inactive compounds for which the docking algorithm had predicted similar or better binding energies. To try to understand the origin of these false positives from docking, the pose for each of the top-ranked 50 compounds was inspected visually. If general problems with the scoring function could be identified, this information could be valuable for further development of the molecular docking algorithm. Two observations were made from this analysis. First of all, there were several cases where polar groups of the fragments or the receptor did not form hydrogen bonds, but were still desolvated to a large extent, which should be energetically unfavorable. Whereas the ligand desolvation is taken into account by the scoring function in DOCK3.6, the receptor desolvation energy contribution is ignored.<sup>37</sup> This may be a reasonable approximation for lead- or drug-like compounds that fill the entire binding site, resulting in a constant desolvation energy contribution. Fragments, on the other hand, often occupy subpockets of the binding site and in these cases the desolvation term could vary significantly and thus be crucial for accurate ranking.<sup>38</sup> The second observation was that there were several top-ranked fragments for which no obvious problems could be identified. Instead, we would likely have predicted several of them to be ligands in a prospective screen against the A<sub>2A</sub>R. To test if any of these were false negatives from the NMR-based screen, we selected five compounds from the top 10% of the ranked library for experimental re-screening in radioligand displacement assays. These five molecules had all been screened by the NMR-based method, but were not among the 94 compounds that were tested in follow-up assays. Three out of five compounds showed >50% displacement of radioligand binding at 500  $\mu$ M. The dose-response curves demonstrated that they were orthosteric ligands with K<sub>i</sub> values equal to 17.6, 20.6 and 128  $\mu$ M (Compounds **6-8**, Table 1). Compound **6** was ranked as number 34 in the docking screen and had the highest LE of all

A<sub>2A</sub>R fragment ligands discovered by docking or NMR ( $LE = 0.56 \text{ kcal mol}^{-1} \text{ atom}^{-1}$ ) and the predicted binding mode for this compound is shown in Figure 3A. Given the potency of these three fragments, it is possible that they have relatively slow off-rates rendering them less sensitive to ligand observed NMR techniques such as TINS.

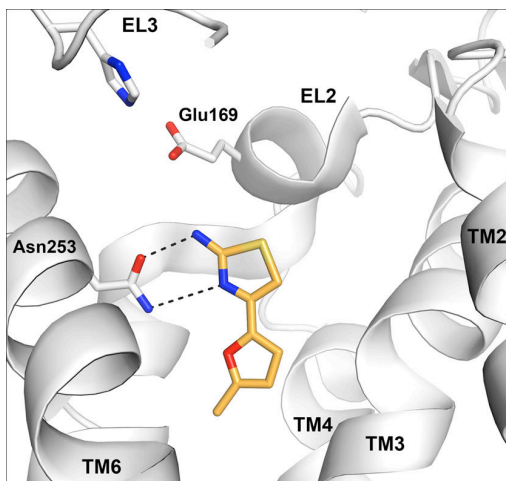


**Figure 3.** Predicted binding mode for a fragment ligand (compound **6**) from the small fragment library that was discovered by docking. The binding site is displayed as a white cartoon with selected side chains shown in sticks. The ligand is depicted with orange carbon atoms. Black dotted lines indicate hydrogen bonds. This figure was generated with PyMOL (version 1.4.1).

### Molecular Docking Screen of Commercially Available Fragments Against an A<sub>2A</sub>R Crystal Structure

Although the positive enrichment of A<sub>2A</sub>R ligands in the fragment library was encouraging, a more interesting test of docking performance would be to extend the number of molecules screened to all commercially available or even all synthetically feasible fragments, e.g. the 166 billion compounds in the GDB-17.<sup>39</sup> One major strength of the *in silico* approach comes from the ability to screen large libraries and reduce the fraction that is tested experimentally to a small number of chemicals. This would enable a more realistic comparison of a typical experimental fragment-based screen to a computational structure-based approach. Screening of a larger chemical library could be also advantageous because of better coverage of chemical space, which gives the opportunity to discover ligand chemotypes that were not available to the NMR-based screen. On the other hand, ranking several hundred thousand disparate fragments by affinity is a tremendous challenge and, as only a few hundred top-ranked

compounds are considered for experimental testing, one may actually expect that molecular docking would perform worse for screening of large chemical libraries.

To test the utility of large-scale docking screens in FBLD, we docked 328,000 commercially available fragments from the ZINC library<sup>40</sup> to an A<sub>2A</sub>R crystal structure using DOCK3.6. The same receptor structure, sampling scheme, and physics-based scoring function as in the first screen were used. The docking of the library was completed in seven hours on 222 cores at a local computer cluster and each molecule was sampled in, on average, 12800 orientations and 40 conformations. The top-ranked 500 compounds, corresponding to 0.15% of the screened library, were considered for experimental testing. There was essentially no overlap of compounds between this set of molecules and the library screened by the NMR-based method. Only one molecule from the small library screened by NMR would have ranked among the top 500 in the docking screen. Twenty-two top ranked molecules from the docking screen of large fragment library (0.007%) were selected for experimental testing based on their complementarity to the orthosteric site and availability from commercial vendors.

The twenty-two predicted fragment ligands were first tested in radioligand assays at 500  $\mu$ M and 14 molecules showed significant radioligand displacement. Subsequent dose-response curves were well behaved (Figure 4), and the K<sub>i</sub> values ranged from 2 to 240  $\mu$ M (Table 2, compounds **9-22**). With the same affinity cut-off as in the NMR-based screen (K<sub>i</sub> < 600  $\mu$ M), the hit-rate from the docking screen was 64%. Although it is difficult to compare screens against different GPCRs, our results were similar to the fragment-based docking campaign against the histamine H<sub>1</sub> receptor, which achieved an unprecedented hit-rate of 73% and identified several potent ligands.<sup>16</sup> Compared to the two previous docking screens of lead-like libraries against the A<sub>2A</sub>R,<sup>10,11</sup> we achieved higher hit-rates, but the affinities of the discovered ligands were typically lower, as expected for fragment screening. To enable a comparison between the hits from our fragment screen and those discovered from docking of lead-like libraries against the same crystal structure, LE values (at 310 K) were calculated for each study. The LE values for the fragments from our *in silico* screen ranged from 0.29

to  $0.56 \text{ kcal mol}^{-1} \text{ atom}^{-1}$  with an average equal to 0.40, which was similar to the results of *Carlsson et al.* ( $0.29\text{--}0.44 \text{ kcal mol}^{-1} \text{ atom}^{-1}$ , average = 0.37)<sup>10</sup> and *Katrich et al.* ( $0.32\text{--}0.52 \text{ kcal mol}^{-1} \text{ atom}^{-1}$ , average = 0.41).<sup>11</sup>

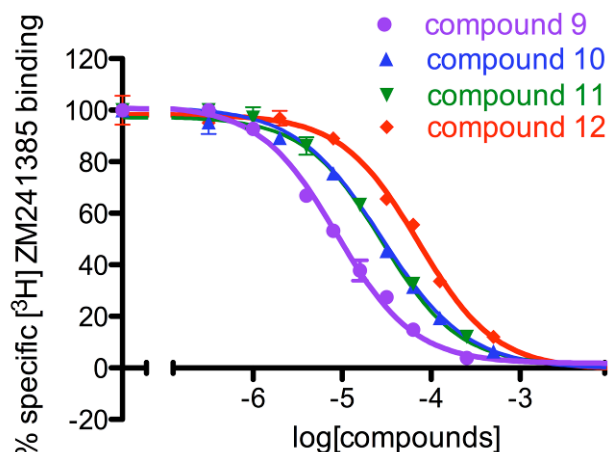


**Figure 4.** Representative concentration-effect curves for displacement of binding of the radiolabeled  $A_{2A}R$  inverse agonist  $[^3H]ZM241385$  by compounds **9**, **10**, **11**, and **12**.

The NMR-based and docking screens are summarized in Figure 5. Five orthosteric ligands were identified in the NMR-based screen, corresponding to a hit-rate of 5% from the secondary screen, and 14 fragment ligands or 64% of those tested experimentally were discovered by docking. Compared to the NMR-based screen, the hits from the  $A_{2A}R$  docking screen had lower  $K_i$  values. Four of the hits from the docking screen were more potent than the compound with the highest affinity from the NMR-based screen. A similar trend was observed for the LE values. Ten compounds from the docking screen had LE values  $>0.35 \text{ kcal mol}^{-1} \text{ atom}^{-1}$ . In comparison, two compounds from the NMR-based screen reached this level. To investigate the novelty of the discovered fragment, we calculated the pairwise Tanimoto similarity with extended chemical fingerprints for four atoms ( $T_c$ , ECFP4) of each hit to the thousands of known  $A_{2A}R$  ligands in the ChEMBL14<sup>41</sup> database. The Tanimoto coefficient ( $T_c$ ) quantifies the two-dimensional chemical similarity between two molecules by a value between 0 and 1. A  $T_c$  value close to zero suggests no chemical similarity between a pair of molecules, whereas a value equal to one represents two identical molecules. For

each discovered ligand, the highest  $T_c$  value among the previously characterized  $A_{2A}R$  ligands is presented in Tables 1 and 2. Some of the hits from the NMR-based and docking screens were relatively similar to known adenosine receptor ligands, e.g. compounds **4** and **9** ( $T_c > 0.4$ ), but in both cases relatively novel chemotypes for the  $A_{2A}R$  were also discovered (e.g. compounds **2**, **5**, **11** and **14**), as reflected by their lower Tanimoto coefficients ( $T_c = 0.28$ - $0.33$ ). Predicted binding modes for compounds **10**, **11**, **12**, and **13** are shown in Figure 6 and 7. As shown in Figure 6, these compounds were predicted to bind deep in the orthosteric binding site. The key interactions for the fragments are hydrogen bonds to Asn253<sup>6.55</sup> and Glu169<sup>5.30</sup> together with  $\pi$ -stacking against the side chain of Phe168<sup>5.29</sup> (superscripts denote Ballesteros-Weinstein numbers<sup>42</sup>), which is consistent with the ligand interactions observed in several of the twelve available  $A_{2A}R$  crystal structures (Figure 7).<sup>6-9</sup>

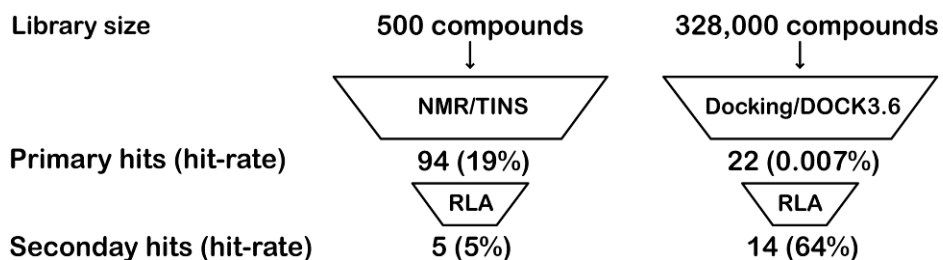


**Figure 5.** Summary of the discovery of orthosteric ligands from the NMR-based and docking screens. Primary screens were carried out using NMR-based (NMR/TINS) and docking (Docking/DOCK3.6) screens. Secondary screens were performed using radioligand binding assays (RLA).

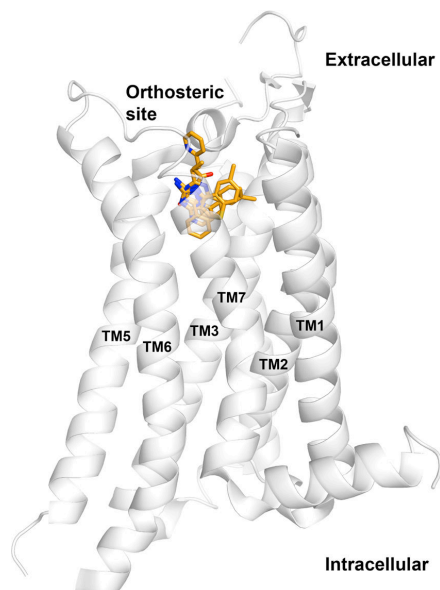


**Figure 6.** Predicted binding modes for compounds **10**, **11**, **12**, and **13** in the orthosteric site of the A<sub>2A</sub>R crystal structure. The A<sub>2A</sub>R is displayed as a white cartoon, and the four ligands are depicted with orange carbon atoms. This figure was generated with PyMOL (version 1.4.1).

### Structure-Activity Relationships and Molecular Dynamics Simulations for Analogs of Compounds **10**, **11**, and **12**

To explore the SAR for the ligands and investigate how the fragments could be further optimized, we docked commercially available analogs of the three potent compounds **10**, **11**, and **12** to the A<sub>2A</sub>R orthosteric site. A series of 23 compounds were selected based on their predicted interactions in the orthosteric site and were tested in radioligand binding assays. Molecular docking in combination with MD simulations was used to guide analog selection and to investigate the predicted binding modes of the screening hits.

Compound **10** was one of the most potent fragment ligands from the screen with a K<sub>i</sub> value of 6.4 μM. The compound also had a promising LE value equal to 0.46 kcal mol<sup>-1</sup> atom<sup>-1</sup>. The binding mode of compound **10** remained stable over one ns of MD simulation with no significant conformational changes in the orthosteric site. The exocyclic amine and triazole group formed strong interactions with Asn253<sup>6.55</sup> in the simulation, whereas the phenyl group was deeply buried in a hydrophobic pocket created by Val84<sup>3.32</sup>, Leu85<sup>3.33</sup>, and Trp246<sup>6.48</sup>. MD simulations of compound **10b** suggested that its substituents that



extended further towards the extracellular loops could be accommodated by the binding pocket. Six analogs of compound **10** were tested to further investigate the binding mode of the ligand (Table 3). Possibilities for optimization of this fragment were first explored by replacing the ethyl with a methyl and propyl substituent (**10a** and **10b**). Reducing the alkyl chain to a methyl led to a 2-fold reduction of affinity, whereas the propyl substituent did not affect the potency. The retention of the potency by the compound with the longer substituent agreed with the predicted interactions with hydrophobic side chains in the opening of the orthosteric site, e.g. Ile274<sup>7.44</sup> and Met270<sup>7.35</sup>. This suggests that further optimization could be achieved by combining **10b** with fragments that extend further toward the extracellular loops. Substitutions on the phenyl ring in the para-position with a methyl-, chlorine-, or methoxy-group led to reductions of the binding affinity in all cases (**10c-e**). The decrease in affinity for the largest substituent was consistent with the prediction that this group was located in an enclosed pocket, in agreement with the predicted binding mode (Figure 7A). Replacing the phenyl group of compound **10b** with a pyridine ring led to a ten-fold decrease in binding affinity to 50  $\mu$ M (**10f**). To investigate the reasons for this large reduction of affinity, we calculated the difference in free energy of binding for these compounds using MD free energy calculations. MD simulations were used to alchemically transform compound **10b** to **10f** in the A<sub>2A</sub>R orthosteric site and in aqueous solution by employing the free energy perturbation (FEP) technique. From these calculations, the difference in binding free energy between the two ligands can be calculated from a thermodynamic cycle.<sup>41</sup> The calculated free energy difference between compounds **10b** and **10f** was  $+1.2 \pm 0.1$  kcal/mol, in close agreement with the experimental 10-fold loss of affinity caused by the pyridine group. Inspection of the MD trajectories suggested that the reason for the calculated reduction of binding affinity was a loss of favorable solvent interactions for the pyridine group in the bound state (Figure 8).

Compound **11** was one of the more novel fragment ligands identified in the docking screen ( $T_c = 0.28$ ) and relatively potent with a  $K_i$  value of 6.3  $\mu$ M. Based on molecular docking and MD simulations of selected fragments, eleven

compounds were selected for experimental testing in radioligand binding assays, which are summarized in Table 4. This congeneric series of fragments explored variations on the pyridine group of compound **11**, which was predicted to interact with residues in the opening of the orthosteric site. Compound **11a**, for which the nitrogen of the pyridine ring was moved to the ortho position, was slightly more potent than the initial hit. On the contrary, replacing the pyridine with a phenyl led to a 3-fold reduction of the  $K_i$  value to 18  $\mu\text{M}$  (**11b**). For compounds **11c-i**, the effects of polar and non-polar substituents on the phenyl ring of compound **11b** were explored. In the ortho-position, polar (**11c**), non-polar (**11d**), and halogen substituents (**11e-f**) improved binding affinity with  $K_i$  values ranging from 5.5 to 8.8  $\mu\text{M}$ . In meta-position, a methyl substituent (**11g**) did not affect affinity relative to compound **11b**, whereas an increase in polarity at this position was found to improve the affinity (**11a**). In para-position, a polar substituent (**11h**) led to a 2-fold improvement of affinity whereas a methyl group was not tolerated and reduced the  $K_i$  value to 60  $\mu\text{M}$  (**11i**). The observed effects on affinity for ortho- and meta- substitutions on the phenyl ring could be explained by the interactions with residues in the opening of the orthosteric site, as this position is close to both polar and non-polar groups in the opening of the orthosteric site. However, the changes in affinity for polar and non-polar substituents in the para-position could not be explained by our model because this position was typically solvent exposed in the predicted binding mode and in the MD simulations (Figure 7B). This may be related to interactions with flexible parts of extracellular loop two, e.g. two rotamers of Glu169<sup>5,30</sup> that have been observed in crystal structures.<sup>6-9</sup> Two additional compounds were designed by combining hydroxyl substituents in ortho- and para-positions with a methoxy group in meta-position (compounds **11j** and **11k**, respectively). The most potent compound, **11k**, had an affinity of 2.4  $\mu\text{M}$ , which is eight-fold better than compound **11b** and a 2-fold improvement compared to the initial hit from the docking screen. The MD simulation of compound **11k** suggested that the methoxy substituent complements the shape of the orthosteric site very well, which is shown in Figure 9.

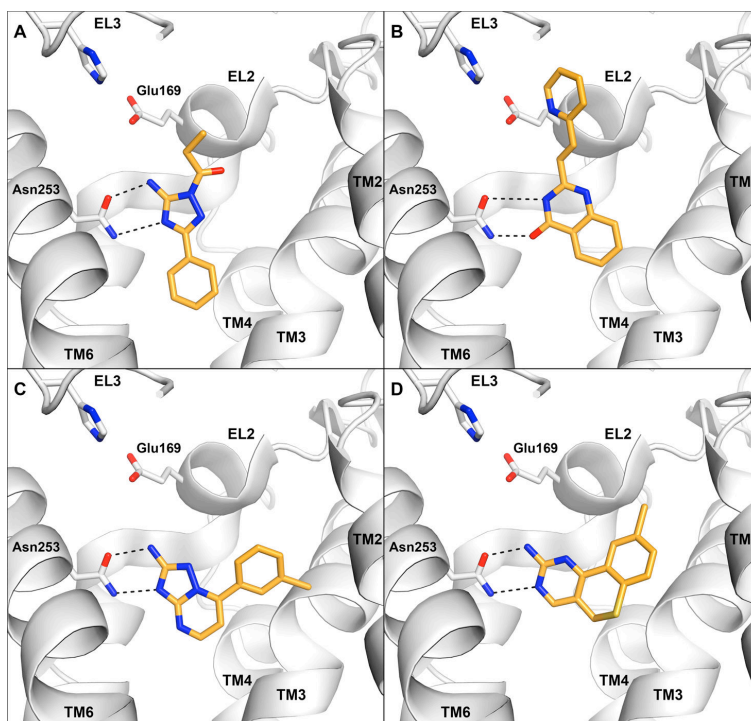


**Figure 7.** Predicted binding modes for four ligands discovered in the molecular docking screen: (A) **10** (B) **11**, (C) **12**, (D) **13**. The binding site is shown in white ribbons with selected side chains shown in sticks. The ligand is depicted with orange carbon atoms. Black dotted lines indicate hydrogen bonds. This figure was generated with PyMOL (version 1.4.1).

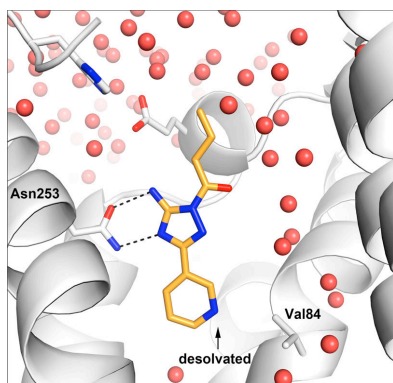


**Figure 8.** Representative molecular dynamics snapshot of the A<sub>2A</sub>R in complex with compound **10f**. The binding site is shown in white ribbons and selected side chains shown in sticks. The ligand is depicted with orange carbon atoms. Water molecules are shown as red spheres. Black dotted lines indicate hydrogen bonds. This figure was generated with PyMOL (version 1.4.1).

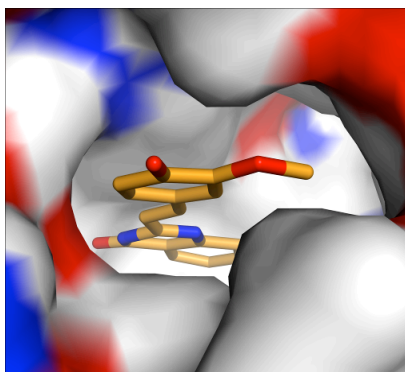
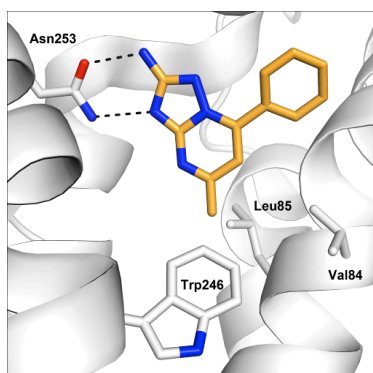


**Figure 9.** Representative snapshot from molecular dynamics simulation of the A<sub>2A</sub>R in complex with compound **11k**. The extracellular part of the A<sub>2A</sub>R is shown in surface representation and the ligand is depicted with orange carbon atoms. This figure was generated with PyMOL (version 1.4.1)

The affinity of compound **12** was 6.8  $\mu\text{M}$  and this fragment had a LE value of 0.43  $\text{kcal mol}^{-1} \text{atom}^{-1}$ . In the predicted binding mode of this ligand, it is almost completely buried in the orthosteric site with the 1,2,4-triazolo[1,5-a]pyrimidine-2-amine group hydrogen bonding with Asn253 and forming stacking interactions with the side chain of Phe168 (Figure 7C). The phenyl group of compound **12** occupied part of the sub-pocket where the ribose ring of  $A_{2A}R$  agonists is located in crystal structures. MD simulations of this fragment suggested that the compound likely explores multiple conformations in the site. In these simulations hydrogen bonds to either Asn253 or Glu169 were conserved, but the phenyl ring explored several subpockets. Six additional compounds in this series were tested experimentally in radioligand binding assays and the results are summarized in Table 5. The compound without any substituents on the phenyl ring was 15-fold less potent than the initial hit,  $K_i = 101 \mu\text{M}$  (**12a**), demonstrating that the Cl in meta-position of compound **12** was essential for binding. In the next step, a Cl in para-position was tested, but this compound was also inactive. Subsequently, a methyl group was added to the pyrimidine group, which resulted in a 50-fold improvement of affinity to 2  $\mu\text{M}$  and an increase of the LE to 0.47  $\text{kcal mol}^{-1} \text{atom}^{-1}$  (**12c**). Substituents in the para-position on the phenyl group on this compound (**12d-f**) did not further improve the affinity of the series. The predicted binding mode for compound **12c** was in good agreement with the observed changes in affinity for the series. The methyl substituent that improved the affinity of compound **12c** to 2.1  $\mu\text{M}$  was positioned in a hydrophobic pocket formed by



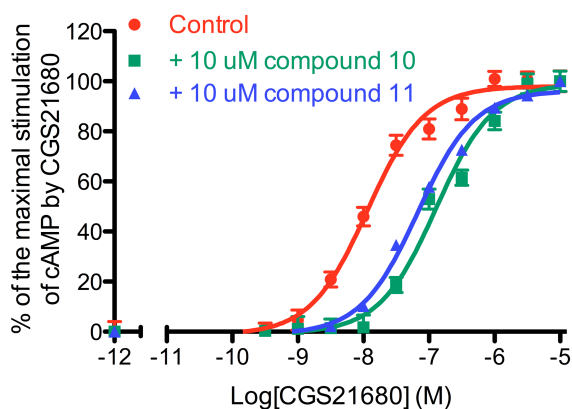
Val84<sup>3,32</sup>, Leu85<sup>3,33</sup>, and Trp246<sup>6,48</sup>. Almost complete burial of the compound in the orthosteric site was likely to be responsible for its high efficiency. (LE=0.47  $\text{kcal mol}^{-1} \text{atom}^{-1}$ , Figure 10)

**Figure 10.** Predicted binding modes for compound **12c**. The binding site is shown in white ribbons with selected side chains shown in sticks. The ligand is depicted with orange carbon atoms. Black dotted lines indicate hydrogen bonds. This figure was generated with PyMOL (version 1.4.1).

## Selectivity and Efficacy for the Discovered Fragment Ligands

One advantage of fragment-based screening is that high hit-rates are often achieved, but the ligands that are discovered are typically not selective for their target. To test the selectivity profile for the fragment ligands that emerged from the *in silico* screen, all compounds were also tested against the A<sub>1</sub>R subtype in radioligand binding assays. Two of the more potent fragments ligands were also tested in cyclic-AMP (cAMP) assays. For the fourteen fragments discovered in the docking screen (Table 2), no significant selectivity for the A<sub>2A</sub>R was found. On the contrary, several ligands actually had better affinities for the A<sub>1</sub>R, with an average 2-fold selectivity for this subtype. The maximal A<sub>1</sub> selectivity among the more potent compounds was a 4-fold difference in affinity for compound **15**. A similar trend was observed for the analogs of compounds **10**, **11**, and **12** (Tables 3, 4, and 5). For the two smaller fragments, **10** and **12**, no significant selectivity for A<sub>2A</sub> over the A<sub>1</sub> subtype was found for any of the analogs. Several of the analogs of compound **11** approached the size of lead-like compounds, and it was also among these compounds that some selectivity for the A<sub>2A</sub>R was observed. The most potent compound in the series (**11k**), had an affinity of 2.4 μM at the A<sub>2A</sub>R, but it was a 4-fold weaker ligand for the A<sub>1</sub> subtype.

Two of the more potent fragments from the docking screen, compounds **10** and **11**, were also tested for their behavior in cAMP assays. Addition of 10 μM of each compound resulted in a rightward shift of the agonist (CGS21680) concentration-effect curve as expected for antagonists (Figure 11). This result is in agreement with previous docking screens of lead-like libraries against A<sub>2A</sub>R



crystal structures in the inactive state that, to our knowledge, only have resulted in the discovery of antagonists.<sup>10,11,44</sup>

**Figure 11.** Functional assay based on measuring the concentration-dependent production of cAMP by A<sub>2A</sub>R agonist CGS21680 for compounds **10** and **11**.

### 3. Discussion

The revolution in GPCR structural biology during the last years has made it possible to take advantage of structure-based methods in ligand discovery against these pharmaceutically important targets. During the same period, FBLD has become widely used in drug discovery, but there are only a few examples of the use of experimental<sup>20,21,45,46</sup> and *in silico*<sup>16,47</sup> fragment screens against GPCRs. To assess the potential benefits of complementing biophysical screens against GPCRs with structure-based discovery of fragment ligands, we carried out two prospective molecular docking screens against the A<sub>2A</sub>R, a drug target for development of drugs against inflammation and Parkinson's disease.<sup>2,3</sup> The parallel screen of a small chemical library against the A<sub>2A</sub>R allowed us to evaluate the ability of molecular docking to distinguish fragment ligands of the receptor. A second comparison was made possible by the large-scale screen of commercially available fragments and subsequent experimental testing of top-ranked compounds.

The first encouraging result was the ability of molecular docking to identify all but one of the hits from the NMR-based screen among the 30 top-ranked compounds. The results are similar to the parallel docking and HTS screen of 200,000 drug-like compounds against Cruzain by *Ferreira et al.*, in which several inhibitors were among the top-ranked compounds.<sup>48</sup> It should be noted that significantly higher enrichment of ligands has been reported by *Katritch et al.* in a benchmark of molecular docking against the same A<sub>2A</sub>R crystal structure.<sup>11</sup> As only lead- to drug-like compounds were used in these retrospective screens, this result could suggest that it is more challenging for docking to identify fragment ligands. However, it could also reflect differences in the scoring functions used and how the non-binders (decoys) were selected. The main finding from the two *in silico* screens that were undertaken in this work was the ability of the molecular docking to complement the biophysical screen for fragment ligands of the A<sub>2A</sub>R. One of the main advantages of fragment-based screening compared to

HTS is that the high hit-rates provide numerous starting points for development of lead compounds.<sup>17,18</sup> However, prioritizing between a large number of primary hits from biophysical screens, a total of 94 from the NMR-based method analyzed here, is often difficult and time-consuming.<sup>21</sup> The successful prediction of the NMR-based screening results strongly suggests that it is advantageous to carry out docking screens in parallel and use the results to select hits for follow-up testing to reduce the number of false positives. This approach would also provide a starting point for structure-based optimization of fragments. Interestingly, a recent comparison between fragment-based screens with different biophysical approaches showed that different sets of ligands are identified using the two methods.<sup>49</sup> To some extent, this likely reflects challenges in detecting low-affinity fragments and suggests that a combination of several orthogonal methods could reduce the number of false negatives and positives from biophysical screens. Our results demonstrate that molecular docking also could play such a role. Several fragments that were top-ranked by docking, but had not been identified by the NMR-based screen, were micromolar ligands with high ligand efficiencies.

The parallel screen also demonstrated major weaknesses of molecular docking screens. As in a majority of all structure-based virtual screens, the receptor volume searched by the docking algorithm was reduced to one pocket on the protein surface. The consequence of this approximation was that allosteric modulators could not be identified. On the contrary, the NMR-based screen led to one of the first discoveries of compounds with positive and negative allosteric effects on ligand binding to the A<sub>2A</sub>R.<sup>2,3</sup> The obvious solution would be to extend the searched volume to include the entire receptor surface, but this would be too computationally expensive for screening of large chemical libraries. Multiple pockets could be considered, but it is not yet clear where the allosteric ligands bind to the A<sub>2A</sub>R, and it would also be a major challenge for docking scoring functions to rank molecules in sites of different sizes and chemical properties. Modulation of receptors via allosteric interactions may provide novel opportunities for development of completely new classes of drugs against the A<sub>2A</sub>R.<sup>50</sup>

The second docking screen unleashed the full potential of the structure-based approach. Several hundred thousand fragments were docked to the A<sub>2A</sub>R crystal structure to identify compounds that complement this receptor conformation. As only a few dozen compounds are evaluated experimentally in this case, more extensive testing can be carried out for each compound, which reduces the risk for false negatives. As in earlier *in silico* screens against A<sub>2A</sub>R and other GPCR crystal structures, the hit-rates were unusually high.<sup>10-16</sup> It may be the combination of a highly ligandable orthosteric site<sup>48</sup> and bias in chemical libraries toward GPCR chemotypes that make structure-based screens against these receptors so successful.<sup>10,12</sup> If this is true, the successes for deep and enclosed binding sites, which are characteristic for the adenosine and aminergic receptors, may not be transferrable to GPCRs with more shallow and solvent exposed pockets. The observation that biophysical screens of fragments generally yield higher hit-rates than those that rely on lead- or drug-like libraries was also demonstrated to be true for *in silico* screens. Several ligands from the docking screen were also more potent than expected from the typical fragment screens, both in comparison to screens against soluble proteins and the NMR-based screen against the same target.<sup>20,21,45</sup>

Successful FBLD relies on the possibility to optimize the initial hits, and, in this step, access to atomic resolution structures provides valuable information. However, in the case of predicting affinities for a series of analogs, subtle structural changes of the receptor may be responsible for differences in potency, which may require a more accurate representation of protein–ligand interactions than molecular docking can provide.<sup>51</sup> Initial attempts to use more rigorous methods in lead optimization of GPCR ligands have been encouraging, and such approaches will likely also play an important role in FBLD against these receptors.<sup>52,53</sup> An increasing amount of computational resources has made it possible to use atomistic simulations to compute the relative affinities for large series of protein–ligand complexes.<sup>54,55</sup> The small size and relatively good availability of force field parameters for fragment-like molecules make them ideal cases for MD simulations and free energy calculations. Here, three new scaffolds



from the *in silico* screen were further explored via analogs and MD simulations of several complexes. The MD simulations provided a deeper understanding of the SAR for analogs of the docking hits, and free energy calculations were used to explain changes in binding affinity due to changes in ligand structure. Two of the scaffolds were optimized to an affinity of 2  $\mu$ M. In particular these compounds, as well as the 15 other discovered fragments that were left unexplored, provide new starting points for development of new lead compounds against this medically important target.

Drug design against GPCRs also involves identifying compounds with a specific efficacy and selectivity profile. The fragments that were tested for efficacy were all antagonists, and this was consistent with that the screen was carried out against a crystal structure in the inactive state. Fragment ligands are typically not selective for their targets, and this is also a general challenge for the A<sub>2A</sub>R because of the strong sequence conservation in the orthosteric site among the four subtypes.<sup>1</sup> None of the ligands discovered in the NMR-based or docking screens showed significant selectivity for A<sub>2A</sub>R over the closely related A<sub>1</sub> subtype, which likely reflected that the fragment hits explored the conserved core of the binding site. If anything, the styryl moiety in compound series **11** had been found as a chemical substructure contributing to A<sub>2A</sub> receptor selectivity before, and indeed in this series there was some selectivity for this receptor subtype too.<sup>56</sup> The refined binding modes for the most potent compounds now provide starting points for optimization of selectivity. In this case, future crystal structures and models of other adenosine receptor subtypes will be crucial for optimizing the selectivity of fragment ligands discovered in biophysical and docking screens.<sup>22,57,58</sup>

## 4. Conclusions

The picture that emerges from this study is that fragment-based ligand discovery via biophysical and computational structure-based screens are highly

complementary approaches. Both the NMR- and molecular docking based screens identified novel A<sub>2A</sub>R fragment ligands with no overlap between the two sets of hits. Molecular docking was shown to be a highly efficient method for the identification of fragments ligands, as reflected by the 64% hit-rate achieved in this screen. On the other hand, the unbiased experimental screen of a relatively small fragment library unexpectedly discovered allosteric modulators of the A<sub>2A</sub>R, which will provide new opportunities for drug development against this receptor. The opportunities to combine biophysical and *in silico* screening methods with structure determination for GPCRs will likely position FBLD as one of the principal approaches for drug development against this pharmaceutically important class of targets.

## 5. Methods

### Molecular Docking Calculations

All docking calculations were carried out with the program DOCK3.6<sup>26-28</sup> using a 2.6 Å resolution crystal structure of the human A<sub>2A</sub>R in complex with an antagonist (PDB accession: 3EML<sup>7</sup>). The receptor was prepared by removing all non-protein atoms and the intracellular T4-lysozyme insertion. The protonation states of ionizable residues of all Asp, Glu, Arg and Lys residues were set to the most probable in aqueous solution at pH 7. The protonation states of the histidines were set by manual inspection (His278<sup>7,43</sup>: protonated in delta position, His250<sup>6,52</sup>: protonated in epsilon position, His264<sup>6,66</sup>: double protonated).

The flexible ligand sampling algorithm in DOCK3.6 superimposes atoms of the docked molecule onto binding site matching spheres, which indicate putative ligand atom positions. Sixty matching spheres were used, and these were either based on the atoms of the crystallographic ligand or positioned manually.<sup>27,28</sup> The spheres were also labeled for chemical matching based on the local receptor environment.<sup>59</sup> The degree of ligand sampling was determined by the bin size, bin size overlap, and distance tolerance. These three parameters were set to 0.4 Å, 0.2 Å, and 1.5 Å, respectively, for both the binding site matching spheres and

the docked molecules. An initial filter discarded conformations that had more than one overlapping heavy atom with the receptor. An overlap between two atoms was defined as a distance shorter than 2.3 and 2.6 Å for polar and non-polar atoms, respectively, and was calculated from a precalculated grid. For ligand conformations passing this steric filter, a physics-based scoring function was used to evaluate the fit to the binding site. For the best scoring conformation of each docked molecule, 100 steps of rigid-body minimization were carried out.<sup>27,28</sup> The score for each conformation was calculated as the sum of the receptor–ligand electrostatic and van der Waals interaction energy, corrected for ligand desolvation. These three terms were evaluated from precalculated grids. The three-dimensional map of the electrostatic potential in the binding site was prepared using the program Delphi.<sup>60</sup> In this calculation, partial charges from the united atom AMBER force field<sup>61</sup> were used for all receptor atoms except the side chain amide of Asn253<sup>6,55</sup>, for which the dipole moment was increased to favor hydrogen bonding to this residue.<sup>10</sup> The program CHEMGRID was used to generate a van der Waals grid, which is based on a united atom version of the AMBER force field.<sup>62</sup> The desolvation penalty for a ligand conformation was estimated from a precalculated transfer free energy of the molecule between solvents of dielectrics 78 and 2. The desolvation energy was obtained by weighting the transfer free energy with a scaling factor that reflects the degree of burial of the ligand in the receptor binding site.<sup>37,63</sup>

Prior to the DOCK3.6 calculation, each docked library was prepared for docking by pre-generating up to 600 conformations using the program OMEGA.<sup>64</sup> Partial atomic charges and transfer free energies were calculated using AMSOL<sup>63,66</sup> and van der Waals parameters were derived from an all-atom AMBER potential.<sup>67</sup> Two libraries were screened. The first was an in-house fragment library of 500 compounds.<sup>31</sup> The second was the ZINC fragment-like library<sup>40</sup> of 328,000 commercially available molecules (molecular weight < 250, LogP < 3.5, and rotatable bonds < 5).

## Similarity Calculations

Similarity calculations for the fragments were carried out using Screenmd program from Chemaxon.<sup>68</sup> We calculated the maximum Tanimoto coefficient with ECFP4 fingerprints between each discovered fragment ligand to the 6509 compounds with recorded activity against the human A<sub>2A</sub>R in the ChEMBL14<sup>41</sup> database.

## Molecular Dynamics Simulations and Free Energy Calculations

The molecular dynamics simulations (MD) and binding free energy calculations for the A<sub>2A</sub>R were performed using a recently published high-resolution crystal structure (PDB accession code: 4EIY<sup>9</sup>, 1.9 Å). In the first step, a hydrated POPC membrane was first equilibrated around the A<sub>2A</sub>R structure without any ligand using periodic boundary conditions in GROMACS<sup>69</sup> using the OPLSAA force field,<sup>70</sup> TIP3P waters,<sup>71</sup> and Berger lipids.<sup>72</sup> In this simulation, all protein atoms were tightly restrained to their initial coordinates, and the hydrated membrane was equilibrated for 40 ns at 300 K. All other MD simulations and free energy calculations of the protein-ligand complexes were carried out starting from the membrane equilibrated A<sub>2A</sub>R system using spherical boundary conditions in the program Q.<sup>73</sup> All ligand force field parameters were obtained using Schrodinger's program hetgrp\_ffgen.<sup>74</sup> The simulations were carried out at a constant temperature of 310 K in a sphere of 18 Å radius centered on the ligand. All protein, water, and ligand atoms within 18 Å of the center of the sphere were explicitly included in the simulations. All atoms outside the sphere were tightly restrained to their initial coordinates and excluded from nonbonded interactions. Asp, Glu, His, Lys, and Arg residues within the spherical system were protonated as in the docking calculation. All other ionizable residues close to the sphere edge or further away than 18 Å were set to their neutral state. The SHAKE<sup>75</sup> algorithm was applied to all solvent bonds and angles and the water molecules at the sphere surface were subjected to radial and polarization restraints.<sup>73,76</sup> A nonbonded cutoff of 10 Å was used for all atoms except the ligand, for which no cutoff was applied. Long-range electrostatic interactions were treated with the

local reaction field (LRF) multipole expansion method.<sup>77</sup> The time step was set to 1 fs, and nonbonded pair lists were updated every 25 steps.

For the docking hits and analogs that were studied with MD simulations, each protein-ligand complex was equilibrated for 810 ps. During the equilibration, harmonic restraints on the protein and ligand atoms were gradually released, which was followed by one ns of unrestrained simulation. To compute the relative free energy of binding from a thermodynamic cycle, the ligands have to be transformed to each other in water and the A<sub>2A</sub>R binding site. The free energy of transforming ligand **10b** to **10f** was computed using the free energy perturbation (FEP) technique, and the calculation was carried out via several intermediates.<sup>78</sup> The potentials governing the intermediate states are defined by  $U_m = \lambda_m U_A + (1 - \lambda_m) U_B$  where  $A$  and  $B$  represent two different ligands, respectively, and  $\lambda_m$  is a mapping parameter which varies from  $\lambda_1 = 0$  to  $\lambda_n = 1$ . The free energy difference between states  $A$  and  $B$  can be calculated by summing up the free energy differences of the  $n$  intermediate states using

$$\Delta G_{A \rightarrow B}^{FEP} = -kT \sum_{m=1}^{n-1} \ln \left\langle e^{-(U_{m+1} - U_m)/kT} \right\rangle_m$$

where  $\langle \dots \rangle_m$  represents an ensemble average on the potential  $U_m$ , which is calculated from MD simulations.<sup>43</sup> The free energy was computed in two steps. First the van der Waals parameters of the phenyl ring of compounds **10b** were transformed to the pyridine of compound **10f**. In a second step, the charges for the same group were changed to those representing pyridine. These calculations were carried out both for the ligand in aqueous solution and in the A<sub>2A</sub>R orthosteric site. The calculations in aqueous solution were carried out by solvating the ligand in a water droplet of radius 18 Å. In these simulations a weak harmonic restraint was applied to keep the ligand close to the center of the sphere. Each FEP calculation comprised a 700 ps heating scheme through eight steps of equilibration. The transformation of partial charges and LJ parameters were carried out with 11  $\lambda$  states (from  $\lambda=0$  to  $\lambda=1$ ) each, with a production run time of 500ps for each lambda point and energies were extracted every 50 steps.

## Cell Culture and Membrane Preparation

HEK293 cells were maintained in culture in DMEM supplemented with 10% newborn calf serum at 37 °C in a moist, 7% CO<sub>2</sub> atmosphere and passaged twice weekly. Cells were transfected with plasmids containing wild-type A<sub>2A</sub>AR construct using the calcium phosphate precipitation method and harvested after 48 hours. Cells were pelleted, re-suspended in 20 ml of ice-cold 50 mM Tris-HCl buffer, pH 7.4. An ULTRA-TURRAX<sup>®</sup> was used to homogenize the cell suspension. The cytosolic and membrane fractions were separated using a high-speed centrifugation step of 100,000 x g for 20 min at 4 °C. This process was repeated twice and subsequently the pellet was re-suspended in 50 mM Tris-HCl buffer, pH 7.4, the protein concentration was determined by the BCA method<sup>79</sup> and samples were aliquoted and stored at - 80 °C until further use.

## Radioligand Binding Studies

Tritiated 4-(2-[7-Amino-2-(2-furyl)-[1,2,4]-triazolo-[2,3-a]-[1,3,5]-triazin-5-yl-amino] ethyl)phenol ([<sup>3</sup>H]ZM241385, specific activity 30 Ci/mmol) and tritiated 1,3-dipropyl-8-cyclopentyl-xanthine ([<sup>3</sup>H]DPCPX, specific activity 120 Ci/mmol) were purchased from ARC Inc. (St. Louis, USA). Unlabelled ZM241385 and -cyclopentyladenosine (CPA) were purchased from Sigma-Aldrich (Steinheim, Germany). The tested compounds were purchased from five different vendors (Asinex, ChemBridge, Vitas-M, Pharmeks and KeyOrganics). The identity of all tested compounds was verified by <sup>1</sup>H-NMR and HPLC/MS was used to assess the purity for all of the molecular docking screening hits.

For the A<sub>2A</sub>Rs, membranes containing 20 µg of protein were incubated in a total volume of 100 µl Tris-HCl buffer (50 mM, pH 7.4), 10 mM MgCl<sub>2</sub>, increasing concentrations of the test compounds (5% DMSO) and [<sup>3</sup>H]ZM241385 at final concentration of 3 nM. Non-specific binding was determined using a final concentration of 10 µM ZM241385 and represented less than 10% of the total binding. For the A<sub>1</sub>Rs, membranes containing 5 µg of protein were incubated in a total volume of 100 µl Tris-HCl buffer (50 mM, pH 7.4), [<sup>3</sup>H]DPCPX (final concentration 1.6 nM) and increasing concentrations of the test compounds (5%

DMSO). Non specific binding was determined using a final concentration of 100  $\mu$ M CPA. Total binding was determined in the presence of buffer and was set at 100% in all experiments, whereas non-specific binding was set at 0%. After incubation for 1 hour at 25 °C in a shaking water bath, assays were terminated by rapid filtration through 96-well GF/B UniFilter plates (PerkinElmer) followed by washing with 7  $\times$  0.25 ml ice-cold Tris-HCl buffer (50 mM, pH 7.4). Plates were dried, 25  $\mu$ l P-E Microscint 20 was added per well, and after 3 hours, bound radioactivity measured using a Packard Microbeta counter (PerkinElmer). Data were analyzed using GraphPad Prism v5, normalized as '% specific binding' from which the  $K_i$  values were calculated. Experiments were performed three times in duplicate, unless stated otherwise.

### **Cyclic AMP Accumulation Assay**

HEK293 cells were grown and transfected as described above. Experiments were performed 48 h after transfection. The cells were harvested and centrifuged two times at 1.000 rpm for 5 min. For cyclic AMP production and determination, 1500 cells/well were used in 384-well Optiplates (PerkinElmer). The cells were incubated for 30 min at 37 °C with either the  $A_{2A}R$  agonist CGS21680 alone or CGS21680 together with test compounds in different concentrations. The assay buffer used was PBS with the addition of 5 mM HEPES, 0.1% BSA, 50  $\mu$ M rolipram, 50  $\mu$ M cilostamide, and 0.8 IU/mL adenosine deaminase. Basal activity was determined in the presence of assay buffer and was set at 0% in all experiments. Maximal receptor activity was determined in the presence of 10  $\mu$ M CGS21680 and was set at 100% in all experiments. Cells were then lysed, and the amount of cAMP produced was quantified using a LANCE ultra cAMP kit (PerkinElmer) according to the instructions of the manufacturer. Following addition of the detection mixture, plates were left for 1 h at RT prior to reading using an EnVision plate reader (PerkinElmer Life Sciences).

## HPLC/MS Protocol

Analytical purity of the compounds **9-15,16-17,19**, and **22** was determined by high-pressure liquid chromatography (HPLC) with a Phenomenex Gemini 3u C18 110A column (50 x 4.6 mm, 3  $\mu$ m), measuring UV absorbance at 254 nm. Sample preparation and HPLC method is - unless stated otherwise - as follows: 0.3-0.8 mg of compound was dissolved in 1 mL of a 1:1:1 mixture of CH<sub>3</sub>CN/H<sub>2</sub>O/tBuOH and eluted from the column within 15 minutes, with a three component system of H<sub>2</sub>O/CH<sub>3</sub>CN/1% TFA in H<sub>2</sub>O, decreasing polarity of the solvent mixture in time from 80/10/10 to 0/90/10.

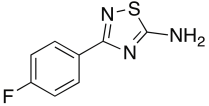
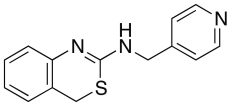
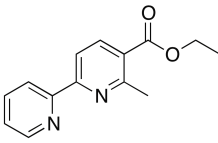
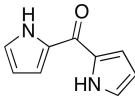
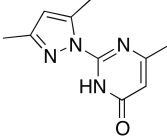
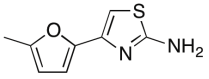
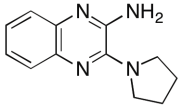
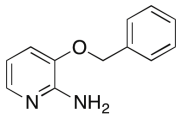
LC-MS analysis was performed on a Finnigan Surveyor HPLC system with a Gemini C18 50 × 4.60 mm column (detection at 200-600 nm), coupled to a Finnigan LCQ Advantage Max mass spectrometer with ESI using the same procedure as mentioned above.

## Contributions

Anirudh Ranganathan and Jen Carlsson (Stockholm University) performed molecule docking screening and molecular dynamics simulations. Jacobus van Veldhoven (LACDR, Leiden) helped for HPLC/MS measurement.



**Table 1.** Fragment ligands and discovered in the NMR-based screen (**1-5**)<sup>21</sup> and false negatives from NMR-screen that were identified by the docking screen (**6-8**).

ID (Rank) <sup>a</sup>	Ligand structure	K <sub>i</sub> (LE <sup>c</sup> ) μM (kcal mol <sup>-1</sup> atom <sup>-1</sup> )	T <sub>c</sub> <sup>d</sup>
1 (26)		14 ± 2.3 (0.53)	0.33
2 (19)		183 ± 20 (0.29)	0.33
3 (7)		324 ± 29 (0.27)	0.39
4 (NS <sup>b</sup> )		472 ± 34 (0.39)	0.42
5 (14)		586 ± 45 (0.31)	0.31
6 (34)		17.6 ± 1.5 (0.56)	0.38
7 (45)		20.6 ± 2.4 (0.42)	0.30
8 (13)		128 ± 11.3 (0.37)	0.44

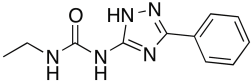
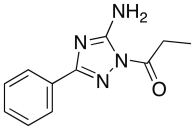
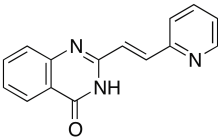
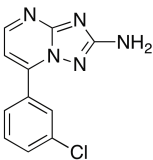
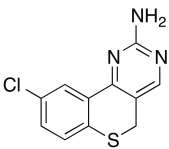
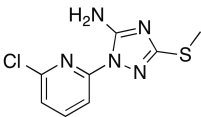
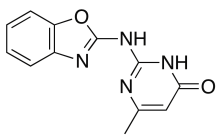
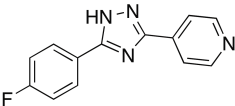
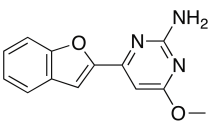
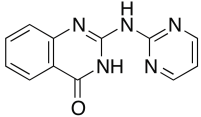
<sup>a</sup> Rank by docking screen of fragment library (500 compounds in total).

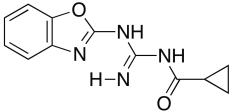
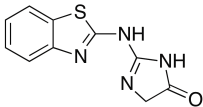
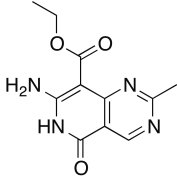
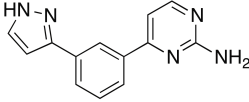
<sup>b</sup> Not scored in molecular docking screen.

<sup>c</sup> Ligand efficiency

<sup>d</sup> Tanimoto similarity (ECFP4 fingerprints) to A<sub>2A</sub> adenosine receptor ligands in the ChEMBL14 database.

**Table 2.** Structures and experimental data for the fragment ligands discovered in the docking screen against the A<sub>2A</sub> adenosine receptor.

ID (Rank) <sup>a</sup>	Ligand structure	K <sub>i</sub> (LE <sup>b</sup> ) $\mu$ M or % displacement at 10 $\mu$ M (kcal mol <sup>-1</sup> atom <sup>-1</sup> )		T <sub>c</sub> <sup>c</sup>
		A <sub>2A</sub>	A <sub>1</sub>	
9 (27)		2.2 $\pm$ 0.2 (0.47)	0.9 $\pm$ 0.1	0.41
10 (348)		6.4 $\pm$ 0.6 (0.46)	4.0 $\pm$ 0.5	0.40
11 (224)		6.3 $\pm$ 0.5 (0.39)	11.1 $\pm$ 1.0	0.28
12 (288)		6.8 $\pm$ 0.4 (0.43)	1.2 $\pm$ 0.3	0.37
13 (468)		16 $\pm$ 3.0 (0.43)	8.0 $\pm$ 0.6	0.31
14 (499)		19.3 $\pm$ 4.2 (0.45)	13 $\pm$ 2	0.28
15 (233)		22.1 $\pm$ 3.1 (0.37)	5.5 $\pm$ 0.5	0.33
16 (386)		29.7 $\pm$ 6.1 (0.36)	22 $\pm$ 2	0.41
17 (235)		33.5 $\pm$ 6.0 (0.35)	10 $\pm$ 2	0.36
18 (10)		39.3 $\pm$ 5.3 (0.35)	7.2 $\pm$ 0.5	0.32

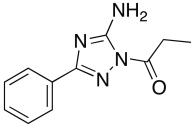
19 (492)		$46.4 \pm 4.7$ (0.34)	$40 \pm 5$	0.37
20 (82)		$95 \pm 5.4$ (0.36)	$80 \pm 4$	0.34
21 (203)		$100 \pm 7$ (0.31)	$104 \pm 8$	0.36
22 (206)		$240 \pm 8$ (0.29)	$173 \pm 6$	0.38

<sup>a</sup> Rank by docking screen of fragment library with 328,000 commercially available compounds.

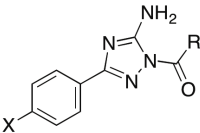
<sup>b</sup> Ligand efficiency

<sup>c</sup> Tanimoto coefficient (ECFP4 fingerprints) to A<sub>2A</sub> adenosine receptor ligands in the ChEMBL14 database.

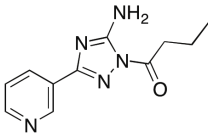
**Table 3.** Structures and experimental data for analogs of compounds **10**.



**10**,  $K_i=6.4 \mu\text{M}$



**10a-e**

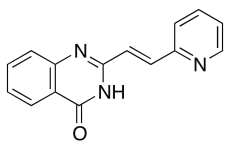


**10f**

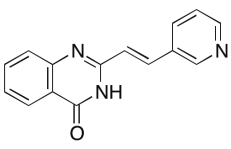
ID	Ligand structure		$K_i$ (LE <sup>a</sup> ) displacement at 10 $\mu\text{M}$ (kcal mol <sup>-1</sup> atom <sup>-1</sup> )	$\mu\text{M}$ or %
	X	R	A <sub>2A</sub>	A <sub>1</sub>
10a	H	CH <sub>3</sub>	11.0 $\pm$ 0.5 (0.47)	11.4 $\pm$ 1.0
10b	H	(CH <sub>2</sub> ) <sub>2</sub> CH <sub>3</sub>	5.1 $\pm$ 0.2 (0.44)	1.0 $\pm$ 0.2
10c	Cl	(CH <sub>2</sub> )CH <sub>3</sub>	17.0 $\pm$ 3.2 (0.40)	44 %
10d	CH <sub>3</sub>	(CH <sub>2</sub> )CH <sub>3</sub>	10.6 $\pm$ 0.6 (0.41)	6.4 $\pm$ 0.3
10e	OCH <sub>3</sub>	(CH <sub>2</sub> ) <sub>2</sub> CH <sub>3</sub>	42 $\pm$ 4 (0.33)	8.1 $\pm$ 0.3
10f	-	-	50 $\pm$ 5 (0.36)	47 %

<sup>a</sup> Ligand efficiency.

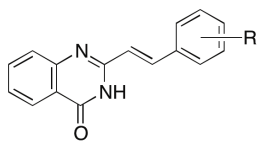
**Table 4.** Structures and experimental data for analogs of compound **11**.



**11**,  $K_i=6.3 \mu\text{M}$



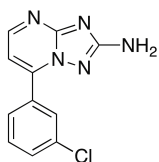
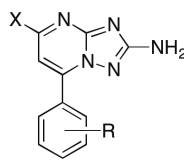
**11a**



**11b-k**

ID	Ligand structure	K <sub>i</sub> (LE <sup>a</sup> ) $\mu\text{M}$ or % displacement at 10 $\mu\text{M}$ (kcal mol <sup>-1</sup> atom <sup>-1</sup> )	
		A <sub>2A</sub>	A <sub>1</sub>
11a	-	4.1 $\pm$ 0.3 (0.40)	20 $\pm$ 2
11b	H	18.0 $\pm$ 1.3 (0.35)	29 %
11c	2-OH	8.8 $\pm$ 0.6 (0.36)	26 %
11d	2-CH <sub>3</sub>	7.8 $\pm$ 0.5 (0.36)	19 %
11e	2-Cl	7.0 $\pm$ 0.4 (0.37)	20 $\pm$ 3
11f	2-F	5.5 $\pm$ 0.3 (0.37)	3.5 $\pm$ 0.4
11g	3-CH <sub>3</sub>	22 $\pm$ 1 (0.33)	24 %
11h	4-OH	7.4 $\pm$ 0.8 (0.36)	34 %
11i	4-CH <sub>3</sub>	60 $\pm$ 5 (0.30)	18 %
11j	2-OH, 3-OCH <sub>3</sub>	9.6 $\pm$ 0.5 (0.32)	25 %
11k	3-OCH <sub>3</sub> , 4-OH	2.4 $\pm$ 0.2 (0.36)	9.6 $\pm$ 0.4

<sup>a</sup> Ligand efficiency

**Table 5.** Structures and experimental data for analogs of compound **12**.**12**  $K_i = 6.8 \mu\text{M}$ **12a-f**

ID	Ligand structure		$K_i$ ( $\text{LE}^a$ ) displacement at $10\mu\text{M}$ ( $\text{kcal mol}^{-1} \text{atom}^{-1}$ )	$\mu\text{M}$ or %
	X	R	$A_{2A}$	$A_1$
12a	H	H	$101 \pm 6$ (0.35)	2 %
12b	H	4-Cl	$99 \pm 5$ (0.33)	17 %
12c	$\text{CH}_3$	H	$2.1 \pm 0.2$ (0.47)	$3.5 \pm 0.3$
12d	$\text{CH}_3$	4- $\text{OCH}_3$	$8.7 \pm 0.1$ (0.40)	$2.8 \pm 0.2$
12e	$\text{CH}_3$	4- $\text{CH}_3$	$3.4 \pm 0.4$ (0.41)	$2.4 \pm 0.3$
12f	$\text{CH}_3$	4-Cl	$9.1 \pm 0.2$ (0.38)	$2.5 \pm 0.2$

<sup>a</sup> Ligand efficiency

## Reference

- (1) Fredholm, B. B.; IJzerman, A. P.; Jacobson, K. A.; Linden, J.; Muller, C. E. International union of basic and clinical pharmacology. LXXXI. Nomenclature and classification of adenosine receptors-an update. *Pharmacol. Rev.* 2011, 63, 1–34.
- (2) Blackburn, M. R.; Vance, C. O.; Morschl, E.; Wilson, C. N. Adenosine receptors and inflammation. *Handb. Exp. Pharmacol.* 2009, 215–269.
- (3) Sebastiao, A. M.; Ribeiro, J. A. Adenosine receptors and the central nervous system. *Handb. Exp. Pharmacol.* 2009, 471–534.
- (4) Katritch, V.; Cherezov, V.; Stevens, R. C. Diversity and modularity of G protein-coupled receptor structures. *Trends Pharmacol. Sci.* 2012, 33, 17–27.
- (5) Congreve, M.; Langmead, C. J.; Mason, J. S.; Marshall, F. H. Progress in structure based drug design for G protein-coupled receptors. *J. Med. Chem.* 2011, 54, 4283–4311.
- (6) Dore, A. S.; Robertson, N.; Errey, J. C.; Ng, I.; Hollenstein, K.; Tehan, B.; Hurrell, E.; Bennett, K.; Congreve, M.; Magnani, F.; Tate, C. G.; Weir, M.; Marshall, F. H. Structure of the adenosine A2A receptor in complex with ZM241385 and the xanthines XAC and caffeine. *Structure* 2011, 19, 1283–1293.
- (7) Jaakola, V. P.; Griffith, M. T.; Hanson, M. A.; Cherezov, V.; Chien, E. Y. T.; Lane, J. R.; IJzerman, A. P.; Stevens, R. C. The 2.6 angstrom crystal structure of a human A2A adenosine receptor bound to an antagonist. *Science* 2008, 322, 1211–1217.
- (8) Lebon, G.; Warne, T.; Edwards, P. C.; Bennett, K.; Langmead, C. J.; Leslie, A. G. W.; Tate, C. G. Agonist-bound adenosine A(2A) receptor structures reveal common features of GPCR activation. *Nature* 2011, 474, 521–525.
- (9) Liu, W.; Chun, E.; Thompson, A. A.; Chubukov, P.; Xu, F.; Katritch, V.; Han, G. W.; Roth, C. B.; Heitman, L. H.; IJzerman, A. P.; Cherezov, V.; Stevens, R. C. Structural basis for allosteric regulation of GPCRs by sodium ions. *Science* 2012, 337, 232–236.
- (10) Carlsson, J.; Yoo, L.; Gao, Z. G.; Irwin, J. J.; Shoichet, B. K.; Jacobson, K. A. Structure-based discovery of A2A adenosine receptor ligands. *J. Med. Chem.* 2010, 53, 3748–3755.
- (11) Katritch, V.; Jaakola, V. P.; Lane, J. R.; Lin, J.; IJzerman, A. P.; Yeager, M.; Kufareva, I.; Stevens, R. C.; Abagyan, R. Structure-based discovery of novel chemotypes for adenosine A2A receptor antagonists. *J. Med. Chem.* 2010, 53, 1799–1809.
- (12) Kolb, P.; Rosenbaum, D. M.; Irwin, J. J.; Fung, J. J.; Kobilka, B. K.; Shoichet, B. K. Structure-based discovery of beta2-adrenergic receptor ligands. *Proc. Natl. Acad. Sci. U. S. A.* 2009, 106, 6843–6848.
- (13) Sabio, M.; Jones, K.; Topiol, S. Use of the X-ray structure of the beta2-adrenergic receptor for drug discovery. Part 2: Identification of active compounds. *Bioorg. Med. Chem. Lett.* 2008, 18, 5391–5395.
- (14) Carlsson, J.; Coleman, R. G.; Setola, V.; Irwin, J. J.; Fan, H.; Schlessinger, A.; Sali, A.; Roth, B. L.; Shoichet, B. K. Ligand discovery from a dopamine D3 receptor homology model and crystal structure. *Nat. Chem. Biol.* 2011, 7, 769–778.
- (15) Mysinger, M. M.; Weiss, D. R.; Ziarek, J. J.; Gravel, S.; Doak, A. K.; Karpiak, J.; Heveker, N.; Shoichet, B. K.; Volkman, B. F. Structure-based ligand discovery for the protein-protein interface of chemokine receptor CXCR4. *Proc. Natl. Acad. Sci. U. S. A.* 2012, 109, 5517–5522.
- (16) de Graaf, C.; Kooistra, A. J.; Vischer, H. F.; Katritch, V.; Kuijer, M.; Shiroishi, M.; Iwata, S.; Shimamura, T.; Stevens, R. C.; de Esch, I. J.; Leurs, R. Crystal structure-based virtual screening for fragment-like ligands of the human histamine H(1) receptor. *J. Med. Chem.* 2011, 54, 8195–8206.
- (17) Congreve, M.; Chessari, G.; Tisi, D.; Woodhead, A. J. Recent developments in fragment-based drug discovery. *J. Med. Chem.* 2008, 51, 3661–3680.
- (18) Hajduk, P. J.; Greer, J. A decade of fragment-based drug design: strategic advances and lessons learned. *Nat. Rev. Drug Discovery* 2007, 6, 211–219.
- (19) Baker, M. Fragment-based lead discovery grows up. *Nat. Rev. Drug Discovery* 2012, 12, 5–7.
- (20) Congreve, M.; Rich, R. L.; Myszka, D. G.; Figaroa, F.; Siegal, G.; Marshall, F. H. Fragment screening of stabilized G-protein-coupled receptors using biophysical methods. *Methods Enzymol.* 2011, 493, 115–136.
- (21) Chen, D.; Errey, J. C.; Heitman, L. H.; Marshall, F. H.; IJzerman, A. P.; Siegal, G. Fragment screening of GPCRs using biophysical methods: identification of ligands of the adenosine A(2A) receptor with novel biological activity. *ACS Chem. Biol.* 2012, 7, 2064–2073.
- (22) Tosh, D. K.; Phan, K.; Gao, Z. G.; Gakh, A. A.; Xu, F.; Deflorian, F.; Abagyan, R.; Stevens, R. C.; Jacobson, K. A.; Katritch, V. Optimization of adenosine 5'-carboxamide derivatives as adenosine receptor agonists using structure-based ligand design and fragment screening. *J. Med. Chem.* 2012, 55, 4297–4308.
- (23) Chen, Y.; Shoichet, B. K. Molecular docking and ligand specificity in fragment-based inhibitor discovery. *Nat. Chem. Biol.* 2009, 5, 358–364.
- (24) Huang, D. Z.; Caflish, A. Library screening by fragment-based docking. *J. Mol. Recognit.* 2010, 23, 183–193.
- (25) Hubbard, R. E.; Chen, I.; Davis, B. Informatics and modeling challenges in fragment-based drug discovery. *Curr. Opin. Drug Discovery Dev.* 2007, 10, 289–297.
- (26) Irwin, J. J.; Shoichet, B. K.; Mysinger, M. M.; Huang, N.; Colizzi, F.; Wassam, P.; Cao, Y. Q. Automated docking screens: a feasibility study. *J. Med. Chem.* 2009, 52, 5712–5720.
- (27) Lorber, D. M.; Shoichet, B. K. Flexible ligand docking using conformational ensembles. *Protein Sci.* 1998, 7, 938–950.
- (28) Lorber, D. M.; Shoichet, B. K. Hierarchical docking of databases of multiple ligand conformations. *Curr. Top. Med. Chem.* 2005, 5, 739–749.
- (29) Magnani, F.; Shibata, Y.; Serrano-Vega, M. J.; Tate, C. G. Co-evolving stability and conformational homogeneity of the human adenosine A2a receptor. *Proc. Natl. Acad. Sci. U. S. A.* 2008, 105, 10744–10749.

- (30) Vanwetswinkel, S.; Heetebrij, R. J.; van Duynhoven, J.; Hollander, J. G.; Filippov, D. V.; Hajduk, P. J.; Siegal, G. TINS, target immobilized NMR screening: an efficient and sensitive method for ligand discovery. *Chem. Biol.* 2005, 12, 207–216.
- (31) Siegal, G.; Ab, E.; Schultz, J. Integration of fragment screening and library design. *Drug Discovery Today* 2007, 12, 1032–1039.
- (32) Kuntz, I. D.; Chen, K.; Sharp, K. A.; Kollman, P. A. The maximal affinity of ligands. *Proc. Natl. Acad. Sci. U. S. A.* 1999, 96, 9997–10002.
- (33) Hopkins, A. L.; Groom, C. R.; Alex, A. Ligand efficiency: a useful metric for lead selection. *Drug Discovery Today* 2004, 9, 430–431.
- (34) Jain, A. N.; Nicholls, A. Recommendations for evaluation of computational methods. *J. Comput.-Aided Mol. Des.* 2008, 22, 133–139.
- (35) Nicholls, A. What do we know and when do we know it? *J. Comput.-Aided Mol. Des.* 2008, 22, 239–255.
- (36) Kim, J.; Wess, J.; van Rhee, A. M.; Schoneberg, T.; Jacobson, K. A. Site-directed mutagenesis identifies residues involved in ligand recognition in the human A2a adenosine receptor. *J. Biol. Chem.* 1995, 270, 13987–13997.
- (37) Mysinger, M. M.; Shoichet, B. K. Rapid context-dependent ligand desolvation in molecular docking. *J. Chem. Inf. Model.* 2010, 50, 1561–1573.
- (38) Majeux, N.; Scarsi, M.; Caffisch, A. Efficient electrostatic solvation model for protein-fragment docking. *Proteins: Struct., Funct., Genet.* 2001, 42, 256–268.
- (39) Ruddigkeit, L.; van Deursen, R.; Blum, L. C.; Raymond, J. L. Enumeration of 166 billion organic small molecules in the chemical universe database GDB-17. *J. Chem. Inf. Model.* 2012, 52, 2864–2875.
- (40) Irwin, J. J.; Sterling, T.; Mysinger, M. M.; Bolstad, E. S.; Coleman, R. G. ZINC: a free tool to discover chemistry for biology. *J. Chem. Inf. Model.* 2012, 52, 1757–1768.
- (41) Gaulton, A.; Bellis, L. J.; Bento, A. P.; Chambers, J.; Davies, M.; Hersey, A.; Light, Y.; McGlinchey, S.; Michalovich, D.; Al-Lazikani, B.; Overington, J. P. ChEMBL: a large-scale bioactivity database for drug discovery. *Nucleic Acids Res.* 2012, 40, D1100–D1107.
- (42) Ballesteros, J. A.; Weinstein, H. Integrated methods for the construction of three-dimensional models of structure–function relations in G protein-coupled receptors. *Methods Neurosci.* 1995, 25, 366–428.
- (43) Kollman, P. Free-energy calculations - applications to chemical and biochemical phenomena. *Chem. Rev.* 1993, 93, 2395–2417.
- (44) Langmead, C. J.; Andrews, S. P.; Congreve, M.; Errey, J. C.; Hurrell, E.; Marshall, F. H.; Mason, J. S.; Richardson, C. M.; Robertson, N.; Zhukov, A.; Weir, M. Identification of novel adenosine A(2A) receptor antagonists by virtual screening. *J. Med. Chem.* 2012, 55, 1904–1909.
- (45) Navratilova, I.; Besnard, J.; Hopkins, A. L. Screening for GPCR ligands using surface plasmon resonance. *ACS Med. Chem. Lett.* 2011, 2, 549–554.
- (46) Stoddart, L. A.; Vernall, A. J.; Denman, J. L.; Bridson, S. J.; Kellam, B.; Hill, S. J. Fragment screening at adenosine-A(3) receptors in living cells using a fluorescence-based binding assay. *Chem. Biol.* 2012, 19, 1105–1115.
- (47) Sirci, F.; Istyastono, E. P.; Vischer, H. F.; Kooistra, A. J.; Nijmeijer, S.; Kuijter, M.; Wijnmans, M.; Mannhold, R.; Leurs, R.; de Esch, I. J.; de Graaf, C. Virtual fragment screening: discovery of histamine h(3) receptor ligands using ligand-based and protein-based molecular fingerprints. *J. Chem. Inf. Model.* 2012, 52, 3308–3324.
- (48) Ferreira, R. S.; Simeonov, A.; Jadhav, A.; Eidam, O.; Mott, B. T.; Keiser, M. J.; McKerrow, J. H.; Maloney, D. J.; Irwin, J. J.; Shoichet, B. K. Complementarity between a docking and a high-throughput screen in discovering new cruzain inhibitors. *J. Med. Chem.* 2010, 53, 4891–4905.
- (49) Wielens, J.; Headey, S. J.; Rhodes, D. I.; Mulder, R. J.; Dolezal, O.; Deadman, J. J.; Newman, J.; Chalmers, D. K.; Parker, M. W.; Peat, T. S.; Scanlon, M. J. Parallel screening of low molecular weight fragment libraries: do differences in methodology affect hit identification? *J. Biomol. Screening* 2013, 18, 147–159.
- (50) Goblyos, A.; IJzerman, A. P. Allosteric modulation of adenosine receptors. *BBA, Biochim. Biophys. Acta, Biomembr.* 2011, 1808, 1309–1318.
- (51) Warren, G. L.; Andrews, C. W.; Capelli, A. M.; Clarke, B.; LaLonde, J.; Lambert, M. H.; Lindvall, M.; Nevins, N.; Semus, S. F.; Senger, S.; Tedesco, G.; Wall, I. D.; Woolven, J. M.; Peishoff, C. E.; Head, M. S. A critical assessment of docking programs and scoring functions. *J. Med. Chem.* 2006, 49, 5912–5931.
- (52) Higgs, C.; Beuming, T.; Sherman, W. Hydration site thermodynamics explain SARs for triazolympurines analogues binding to the A2A receptor. *ACS Med. Chem. Lett.* 2010, 1, 160–164.
- (53) Dror, R. O.; Pan, A. C.; Arlow, D. H.; Borhani, D. W.; Maragakis, P.; Shan, Y. B.; Xu, H. F.; Shaw, D. E. Pathway and mechanism of drug binding to G-protein-coupled receptors. *Proc. Natl. Acad. Sci. U. S. A.* 2011, 108, 13118–13123.
- (54) Carlsson, J.; Boukharta, L.; Aqvist, J. Combining docking, molecular dynamics and the linear interaction energy method to predict binding modes and affinities for non-nucleoside inhibitors to HIV-1 reverse transcriptase. *J. Med. Chem.* 2008, 51, 2648–2656.
- (55) Jorgensen, W. L. Efficient drug lead discovery and optimization. *Acc. Chem. Res.* 2009, 42, 724–733.
- (56) Jacobson, K. A.; Gallo-Rodriguez, C.; Melman, N.; Fischer, B.; Maillard, M.; van Bergen, A.; van Galen, P. J.; Karton, Y. Structure–activity relationships of 8-styrylxanthines as A2-selective adenosine antagonists. *J. Med. Chem.* 1993, 36, 1333–1342.
- (57) Katritch, V.; Kufareva, I.; Abagyan, R. Structure based prediction of subtype-selectivity for adenosine receptor antagonists. *Neuro-pharmacology* 2011, 60, 108–115.
- (58) Kolb, P.; Phan, K.; Gao, Z. G.; Marko, A. C.; Sali, A.; Jacobson, K. A. Limits of ligand selectivity from docking to models: in silico screening for A(1) adenosine receptor antagonists. *PloS One* 2012, 7, e49910.
- (59) Shoichet, B. K.; Kuntz, I. D. Matching chemistry and shape in molecular docking. *Protein Eng.* 1993, 6, 723–732.
- (60) Nicholls, A.; Honig, B. A rapid finite-difference algorithm, utilizing successive over-relaxation to solve the Poisson-Boltzmann equation. *J. Comput. Chem.* 1991, 12, 435–445.



- (61) Weiner, S. J.; Kollman, P. A.; Case, D. A.; Singh, U. C.; Ghio, C.; Alagona, G.; Profeta, S.; Weiner, P. A new force-field for molecular mechanical simulation of nucleic-acids and proteins. *J. Am. Chem. Soc.* 1984, 106, 765–784.
- (62) Meng, E. C.; Shoichet, B. K.; Kuntz, I. D. Automated docking with grid-based energy evaluation. *J. Comput. Chem.* 1992, 13, 505–524.
- (63) Shoichet, B. K.; Leach, A. R.; Kuntz, I. D. Ligand solvation in molecular docking. *Proteins: Struct., Funct., Genet.* 1999, 34, 4–16.
- (64) Omega, OpenEye Scientific Software v 2.3.2; 2008. [www.eyesopen.com](http://www.eyesopen.com).
- (65) Chambers, C. C.; Hawkins, G. D.; Cramer, C. J.; Truhlar, D. G. Model for aqueous solvation based on class IV atomic charges and first solvation shell effects. *J. Phys. Chem.* 1996, 100, 16385–16398.
- (66) Li, J. B.; Zhu, T. H.; Cramer, C. J.; Truhlar, D. G. New class IV charge model for extracting accurate partial charges from wave functions. *J. Phys. Chem. A* 1998, 102, 1820–1831.
- (67) Weiner, S. J.; Kollman, P. A.; Nguyen, D. T.; Case, D. A. An all atom force-field for simulations of proteins and nucleic-acids. *J. Comput. Chem.* 1986, 7, 230–252.
- (68) JChem, Chemaxon, v 5.11.4; 2012. <http://www.chemaxon.com>.
- (69) Hess, B.; Kutzner, C.; van der Spoel, D.; Lindahl, E. GROMACS 4: algorithms for highly efficient, load-balanced, and scalable molecular simulation. *J. Chem. Theory Comput.* 2008, 4, 435–447.
- (70) Jorgensen, W. L.; Maxwell, D. S.; TiradoRives, J. Development and testing of the OPLS all-atom force field on conformational energetics and properties of organic liquids. *J. Am. Chem. Soc.* 1996, 118, 11225–11236.
- (71) Jorgensen, W. L.; Chandrasekhar, J.; Madura, J. D.; Impey, R. W.; Klein, M. L. Comparison of simple potential functions for simulating liquid water. *J. Chem. Phys.* 1983, 79, 926–935.
- (72) Berger, O.; Edholm, O.; Jahnig, F. Molecular dynamics simulations of a fluid bilayer of dipalmitoylphosphatidylcholine at full hydration, constant pressure, and constant temperature. *Biophys. J.* 1997, 72, 2002–2013.
- (73) Marelus, J.; Kolmodin, K.; Feierberg, I.; Aqvist, J. Q. A molecular dynamics program for free energy calculations and empirical valence bond simulations in biomolecular systems. *J. Mol. Graphics Modell.* 1998, 16, 213–225.
- (74) Hetgrp\_ffgen, Schrodinger, 2011. <http://www.schrodinger.com>.
- (75) Ryckaert, J. P.; Ciccotti, G.; Berendsen, H. J. C. Numerical- integration of Cartesian equations of motion of a system with constraints - molecular-dynamics of N-alkanes. *J. Comput. Phys.* 1977, 23, 327–341.
- (76) King, G.; Warshel, A. A surface constrained all-atom solvent model for effective simulations of polar solutions. *J. Chem. Phys.* 1989, 91, 3647–3661.
- (77) Lee, F. S.; Warshel, A. A local reaction field method for fast evaluation of long-range electrostatic interactions in molecular simulations. *J. Chem. Phys.* 1992, 97, 3100–3107.
- (78) Brandsdal, B. O.; Osterberg, F.; Almlöf, M.; Feierberg, I.; Luzhkov, V. B.; Aqvist, J. Free energy calculations and ligand binding. *Adv. Protein Chem.* 2003, 66, 123–158.
- (79) Smith, P. K.; Krohn, R. I.; Hermanson, G. T.; Mallia, A. K.; Gartner, F. H.; Provenzano, M. D.; Fujimoto, E. K.; Goeke, N. M.; Olson, B. J.; Klenk, D. C. Measurement of protein using bicinchoninic acid. *Anal. Biochem.* 1985, 150, 76–85.

